Published in final edited form as:
Biochemistry. 2007 December 11; 46(49): 14188–14197. doi:10.1021/bi701363s.

The Role of Y94 in Proton and Hydride Transfers Catalyzed by Thymidylate Synthase†

Baoyu Hong[§,^], **Frank Maley**[#], and **Amnon Kohen**[§*]

§*Department of Chemistry, University of Iowa, Iowa City, IA 52242*

#*Wadsworth Center, New York State Dept. of Health, Albany, NY 12201*

Abstract

Thymidylate synthase (TS) catalyzes the substitution of a carbon-bound proton in a uracil base by a methyl group to yield thymine in the de novo biosynthesis of this DNA base. The enzymatic mechanism involves making and breaking several covalent bonds. Traditionally, a conserved tyrosine (Y94 in *E. coli*, Y146 in *L. casei*, and Y135 in human) was assumed to serve as the general base catalyzing the proton abstraction. That assumption was examined here by comparing the nature of the proton abstraction using wild type (*wt*) *E. coli* TS (*ec*TS) and its Y94F mutant (with a two orders of magnitude reduced turnover rate). A subsequent hydride transfer was also studied using the *wt* and Y94F. The physical nature of both H-transfer steps was examined by determining intrinsic kinetic isotope effects (KIEs). Surprisingly, the findings did not suggest a direct role for Y94 in the proton abstraction step. The effect of this mutation on the subsequent hydride transfer was examined by a comparison of the temperature dependency of the intrinsic KIE on both the *wt* and the mutant. The intrinsic KIEs for Y94F at physiological temperatures were slightly smaller than for *wt*, but otherwise, were as temperature independent, suggesting a perfectly pre-organized reaction coordinate for both enzymes. At reduced temperature, however, the KIE for the mutant increased with decreasing temperature, indicating a poorly pre-organized reaction coordinate. Other kinetic and structural properties were also compared and the findings suggested that Y94 is part of a H-bond network that plays a critical role at a step between the proton and the hydride transfers, presumably the dissociation of H_4folate from the covalently bound intermediate. The possibility that no single residue serves as the general base in question, but rather, that the whole network of H-bonds at the active site catalyzes proton abstraction, is discussed.

Thymidylate synthase (TS) catalyzes the reductive methylation of 2'-deoxyuridylate (dUMP) with 5,10-methylene−5, 6, 7, 8-tetrahydrofolate (CH_2H_4folate), forming thymidine monophosphate (dTMP) and 7, 8-dihydrofolate (H_2folate) (1). TS activity is essential to living organisms since it catalyzes the de novo synthesis of one of the DNA building blocks. Consequently, TS is a common target in cancer chemotherapy, antibiotic drugs, and gene therapy (2,3). The TS-catalyzed reaction has been elucidated in detail by a wide variety of kinetic, genetic, and structural methodologies (1,4–6), which have shown that TS is a homo-dimer utilizing a half-of-the-sites-activity mechanism (7,8). Steady state measurements indicated a bi-bi ordered mechanism with substrate (dUMP) binding before the CH_2H_4folate (4,9). Kinetic and structural studies identified coherent protein motion that appear coupled to a hydride transfer step (10,11), which is rate limiting for the *wt* TS.

†This work was supported by NIH R01 GM65368-01 and NSF CHE- 0133117 to A.K.

*Address correspondence to this author: Tel: 319-335-0234. Fax: 319-335-1270, Email: amnon-kohen@uiowa.edu.
^Current address: The Department of Pharmaceutical Chemistry, School of Pharmacy, University of California, San Francisco, San Francisco, CA, 94158-2517

Scheme 1 illustrates the two main variations proposed for the chemical mechanisms along the complex cascade of TS catalysis. In the traditional proposed mechanism (1,4), E58 assists in the formation of an iminium ion (A in scheme 1), which is is subjected to nucleophilic attack by the C5 enolate of the C146-activated dUMP (12) to form a ternary intermediate (C). A proton is then abstracted from C5 of dUMP to form the enol D (step 4) (4). This is followed by the release of H_4folate from the ternary complex (step 5, E1CB mechanism) (13) to generate the exocyclic methylene intermediate (E). Finally, the product dTMP is formed in step 6 by hydride transfer from (6*S*)-H_4folate to the exocyclic methylene of the enzyme-bound nucleotide via a 1,3-S_N2 mechanism. Several experimental studies indicate that this last step is the overall rate limiting step for both first order rate constant, k_{cat}, and second order rate constant, k_{cat}/K_M (depicted below as *V/K*) (10,14,15). Recently, QM/MM calculations (16) suggested an alternative path with lower activation energies. In the new path, the keto-enol tautomerization at C4 of dUMP plays a minor role while the labile C6-S-Cys bond plays a major role. The differences from the traditional mechanism are: (i) Steps 2 and 3 occur concertedly; (ii) The abstraction of the proton from the C5 of dUMP involves E2 elimination of C146 (step 4'), and (iii) The dissociation of CH_2H_4folate occurs via 1,3-S_N2 substitution with thiolate of C146 as the nucleophile and N5 of H_4folate as the leaving group (step 5').

The proton abstraction from position 5 of the pyrimidine ring is crucial in the breakdown of the ternary intermediate and is the focus of this work. The general base in the active site has been proposed to be Y94 (see ref (4) and many cited therein). Figure 1 presents the crystal structure of the *wt E. coli* TS with covalently bound dUMP and non-covalently bound folate analogue at the active site (PDB # 2KCE). The water molecule (W608) is located 2.6 Å from the oxygen of Y94 and 3.6 Å from the C5 of dUMP, and was assumed to serve as the initial acceptor of the abstracted proton in step 5 (4,13,17–19). Hardy et al. (20) proposed that the general base in step 4 is N5 of the H_4folate through an "H-wire", using water as conduit. Mutagenesis studies (19) demonstrated that several modifications of Y94 lead to loss of activity. This fact was interpreted as support of a mechanism in which Y94 assists in the proton abstraction. These issues are further examined in the current paper.

Another interesting feature of the current work is that no isotope effects have been measured on the C5-H bond cleavage, which is not a rate limiting step for any measurable rate constant. Previous measurements monitored the ratio of ^3H to ^{14}C using [2-^{14}C, 5-^3H] dUMP as a substrate with a saturating CH_2H_4folate concentration and reported no KIE (unity) or even a slightly inverse KIE (4). The reason for the inverse KIEs is likely to be a fast and reversible exchange of the C5 proton through steps 1–4, prior to the irreversible and rate limiting hydride transfer in step 6. Furthermore, the high concentration of CH_2H_4folate, which binds after dUMP binds (4,5), would mask a possible intrinsic KIE if the isotopic label is on the substrate (20–24). In the current work, the KIEs on this proton abstraction were studied as a function of the concentration of CH_2H_4folate in combination with the Northrop method (25–28). The observed KIEs versus the CH_2H_4folate concentration clearly indicated a kinetic mechanism with ordered substrate binding for the *wt* and less ordered binding for Y94F. A comparison of the intrinsic KIEs of the mutant and the *wt* served as a probe for the role of Y94 in this step.

Additionally, we investigated the effect of altering the hydrogen bond network at the active site by Y94F mutation and the nature of another chemical transformation remote from Y94, namely the hydride transfer (step 6 in scheme 1). The comparison of the temperature dependency of the intrinsic KIEs and activation parameters of Y94F with that of *wt* (10) indicated a minor effect of this mutation at physiological temperature, but a substantial distortion of the reaction's pre-organization at reduced temperature. Together, the examination of the effect of Y94F on the proton abstraction (step 4 or 4') and on the hydride transfer (step 6) indicated that a more likely role of Y94 is in the protonation of the N5 of H_4folate (the leaving group in step 5 or 5'), as discussed in detail below.

MATERIALS AND METHODS

Materials

[2-^{14}C] dUMP (specific radioactivity 52 Ci/mol) and [5-^{3}H] dUMP (specific radioactivity 13.6 Ci/mmol) were from Moravek Biochemicals. [^{2}H] $NaBH_4$ (> 99.5% D) was from Cambridge Isotopes. [^{3}H] $NaBH_4$ (15 Ci/mmol) was from American Radiolabeled Chemicals. Dihydrofolate (H_2folate) was synthesized following the procedure of Blakley (29). [2-^{3}H] iPrOH was prepared by reduction of acetone with [^{3}H] $NaBH_4$ (specific radioactivity of 15 Ci/mmol) as described in detail elsewhere (30). All other materials were purchased from Sigma.

Synthesis of [2- ^{14}C, 5-D] dUMP (> 99.5% D)—[2- ^{14}C, 5-D] dUMP was prepared by modifying the method of Wataya and Hayatsu (31–33) using L-cysteine in D_2O to catalyze H to D exchange at the C5 position of [2-^{14}C] dUMP. The reaction was conducted by incubation of [2-^{14}C] dUMP (~1mM and 52mCi/mmol) in a D_2O solution (> 99.9% D) containing 1 M of L-cysteine at 37°C and a pD of 8.8 for 7 days. The reaction was carried to completion as determined by ^{1}H NMR.

Synthesis of Isotopically C6 Labeled CH_2H_4folate for Measurement of KIE on Hydride Transfer—The synthesis of (*R*)-[6-^{3}H] CH_2H_4folate was performed through a combination of two enzymatic reactions as described previously (30). Briefly, [2-^{3}H]iPrOH was prepared by reduction of acetone with [^{3}H]$NaBH_4$. $NADP^+$ was reduced by [2-^{3}H]iPrOH to (*R*) –[4-^{3}H] NADPH by alcohol dehydrogenase from *Thermoanaerobium brockii* (*tb*ADH). DHFR catalyzed the *in situ* conversion of H_2folate to (*S*)-[6-^{3}H] H_4folate using (*R*) –[4-^{3}H] NADPH and then the isotopically labeled H_4folate was converted to (*R*)-[6-^{3}H] CH_2H_4folate upon quenching with formaldehyde. Similarly, the mixture of (*R*)-[6-^{3}H] CH_2H_4folate and (*R*)-[6-^{2}H]- CH_2H_4folate for the D/T KIE measurement was synthesized under same condition with the mixture of D- and T- labeled isopropanols. The radioactively labeled CH_2H_4folate was purified by reverse phase HPLC, lyophilized and stored at −80 °C prior to use.

Enzyme

Wild-type *E. coli* TS was prepared and purified according to the procedure of ref (34). Y94F was prepared and purified as described in detail elsewhere (6,13,19). The mutant was stored as ammonium sulfate pellets at −80 °C and prior to use, was dissolved and dialyzed against a mixture of 25 mM potassium phosphate, 10% ethylene glycol and 2 mM DTT. *tb*ADH was purchased from Sigma.

Methods

Competitive and Intrinsic Primary Kinetic Isotope Effect (1 °KIE) for C5 Proton Abstraction—The 1° KIEs on proton abstraction from the 5 position of the dUMP were measured competitively. The reaction mixture contained 50 mM β-mercaptoethanol, 1 mM EDTA and 5 mM formaldehyde in 100 mM Tris buffer (pH 7.5). Prior to kinetic assay, 1.5 Mdpm [5-^{3}H] dUMP, 0.5 Mdpm of [2-^{14}C] dUMP and varied concentrations of CH_2H_4folate (2 μM to1000 μM) were added to the buffer mixture at 25 °C. The reaction was initiated by adding enzyme (*wt* or Y94F TS). Five aliquots of 100 μL were removed at different time points (t), quenched with 30 μM 5-fluoro-2'-deoxyuridine-5'-monophosphate (F-dUMP, a nM inhibitor of TS). Then, a concentrated solution of *wt* TS was added to the reaction mixture to a final concentration of 0.1 mM, followed by 10 more minutes of incubation to complete the reaction (t∞). Two t_0s (reaction mixture prior to adding enzyme and used as control) and three t∞s were obtained for each experiment and independent experiments were performed in triplicate. All the quenched samples were stored in dry ice before HPLC analysis. The method of RP HPLC separation and liquid scintillation counter (LSC) analysis of the ^{3}H/^{14}C ratio is described in detail elsewhere (30).

The competitive observed KIEs on the second order rate constant *V/K* were determined using the following equation (35):

$$\mathrm{KIE}=\frac{\ln(1-f)}{\ln\left(1-f\cdot\frac{R_t}{R_\infty}\right)} \quad [1]$$

where *f* is the fractional conversion to product dTMP (typically ranging from 20 to 80 %), R_t and R∞ are ratio of $^3H/^{14}C$ in products (water and dTMP) at each time point and time infinity. The fractional conversion *f* was calculated by:

$$f=\frac{[^{14}C]\mathrm{dTMP}}{[^{14}C]\mathrm{dTMP}+[^{14}C]\mathrm{dUMP}} \quad [2]$$

Figure 2 presents an example of measured H/T KIEs as function of *f*. Since the KIE on the proton abstraction has not been measured before, it is important to demonstrate that the KIE is reproducible in a series of independent experiments and that there is no upward or downward trends in the KIE as function of *f*.* Figure 3 presents the observed H/T KIEs of the mutant and the *wt* as a function of CH_2H_4folate concentration. The analysis of the observed KIEs on the proton abstraction as function of CH_2H_4folate is presented under Results and Discussion.

To determine the intrinsic KIE for this step, 5 μM CH_2H_4folate was used to measure the observed H/T and D/T KIEs. The observed D/T KIE was measured using the exact same conditions as that for the H/T KIE except the [2-^{14}C] dUMP was replaced by [2-^{14}C, 5-D] dUMP. So, the ^{14}C now represents the D-transfer rather than H-transfer. Intrinsic KIEs are calculated from equation 3, (25–28):

$$\frac{{}^{T}(V/K)^{-1}_{\mathrm{H\ obs}}-1}{{}^{T}(V/K)^{-1}_{\mathrm{D\ obs}}-1}=\frac{k_T/k_H-1}{(k_T/k_H)^{1/3.34}-1} \quad [3]$$

where ${}^{T}(V/K)_{\mathrm{H,\ obs}}$ and ${}^{T}(V/K)_{\mathrm{D,\ obs}}$ are the observed competitive H/T and D/T KIEs; k_T/k_H represents the reciprocal of k_H/k_T (intrinsic H/T KIE). Although the intrinsic H/T KIE is the only unknown in this equation, it cannot be solved analytically. Therefore, a program has been developed to solve this equation numerically (now available free of charge at: http://cricket.chem.uiowa.edu/~kohen/tools.html). Since error propagations in this case cannot be conducted analytically from derivatization of Eq. 3, the intrinsic KIEs were analyzed by calculation the intrinsic KIEs from independent and random combinations of observed H/T and D/T KIEs (36). The Northrop method for a reversible step assumes ${}^{T}K_{eq}$ close to unity (25–27). We measured the ${}^{D}K_{eq}$ using the Cys activated dUMP as model compound for intermediate C in Scheme 1 (as described in the following item), and found it to be unity within experimental error. Additionally, the ${}^{T}K_{eq}$ for the proton abstraction can be estimated to be close to unity from fractionation factors for protons bound to similar carbons, and the fractionation factor in the product water molecule being unity since water is the reference system (37). Finally, since the reverse step in question involves the competition of tritium and protons from water, as discussed below, even a larger EIE should have little effect on the outcome of the Northrop method.

Equilibrium Isotope Effect (EIE) on activated dUMP—To assess the EIE (${}^{D}K_{eq}$) on the proton abstraction on C5 of dUMP, we used a model in which C6 is activated by high concentration of Cys in solution. The activated complex was allowed to exchange with 50 % H_2O/D_2O. Specifically, 270 mM dUMP and 1 M of L-cysteine were incubated in 50 % H_2O/D_2O (mol/mol) at 37 °C and a pH of 8.8 for 5, 7, and 9 days. The progress of the exchange reaction was monitored by ^{1}H-NMR until completion (no further change in H content at C5).

*Most artifacts in a competitive experiment will result in such a trend.

For an accurate NMR examination, the samples were lyophilized and redissolved in pure D_2O at a pD of 1.5 (the exchange reaction does not proceed at this pD). Then, the ratio between the hydrogen on C6 (unexchangeable) and the one on C5 was determined by ^{1}H-NMR. The hydrogen on C3' was used as integration reference of unity and the H6/H5 ratio was determined in quintuplets. The H5/H6 values were 0.510 (±0.008) /1.010 (±0.007) indicating $^{D}K_{eq}$ = 0.99 (±0.02) for the proton exchange with water. [*].

Competitive and Intrinsic Primary Kinetic Isotope Effect (1 °KIE) on Hydride Transfer from C6 (Step 6 in Scheme 1)—The competitive H/T and D/T KIEs for the hydride transfer from the 6 position of CH_2H_4folate with Y94F mutant were measured using the same conditions as with the *wt* TS (10). In short, the reaction mixture contains 1.5 Mdpm tritiated *R*- [6 - ^{3}H] CH_2H_4folate for the H/T KIE or deuterated *R*-[6-^{2}H] CH_2H_4folate for the D/T KIE, respectively, 0.5 Mdpm [2-^{14}C] dUMP, 50 mM β-mercaptoethanol, 1 mM EDTA and 5 mM of formaldehyde in 100 mM Tris buffer with a pH of 7.5 (adjusted at each experimental temperature). About 30 % molar excess of dUMP was used in the reaction mixture in order to ensure 100 % conversion of tritiated CH_2H_4folate at time infinity (essential for R∞- see below). The reaction mixture was pre-incubated at the respective experimental temperatures and initiated by adding Y94F. At five different time points, 100 μL aliquots were removed and quenched with 30 μM F-dUMP. Concentrated *wt* TS was added to the reaction mixture to achieve 100% conversion (t∞). Two t_0s (used as quality control) and three t∞s were obtained for each experiment and independent experiments were performed in at least duplicate. The competitive observed KIEs were determined by Eq. 1 and the fractional conversion *f* was determined from equation 4 (30):

$$f = \frac{[^{14}C]\text{dTMP}}{(100 - \%_{\text{excess}}) \cdot ([^{14}C]\text{dTMP} + [^{14}C]\text{dUMP})} \quad [4]$$

where % excess = [(total ^{14}C) − ([2- ^{14}C] dTMP)∞]/(total ^{14}C).

The intrinsic H/T and D/T KIEs are calculated from Eq. 3 with the error propagation processed in that same as was for the aforementioned proton abstraction step. The analysis of these data is described in Result and Discussion, below.

Steady-State Kinetics—The initial velocities were measured under steady state conditions in a buffer mixture containing 50 mM DTT, 5 mM formaldehyde, 1 mM EDTA, and 100 mM Tris with a pH of 7.5 (adjusted at each experimental temperature). The reaction was monitored by following the increase of absorbance at 340 nm upon conversion of CH_2H_4folate to H_2folate ($\Delta\varepsilon_{340nm}$ = 6.4 $mM^{-1}cm^{-1}$) (14). The individual reaction mixture was pre-equilibrated at experimental temperatures and initiated by adding enzyme. Each measurement was conducted at least in duplicate and the data were analyzed as described in Results and Discussions.

RESULTS AND DISSCUSSION

Structural Comparison

A recent X-ray crystallography study (38) examined the Y94F mutant at 1.6 Å and 2.0 Å resolution (without and with ligands, respectively). An overlap of crystal structures of the *wt* and the mutant (Figure 4) indicates a perfect overlap, including electron density for defined water molecules (r.m.s.d. = 0.014 Å (38)). The obvious exception is the lack of the hydroxyl at residue 94 and the water molecule that is hydrogen bonded to the OH group in the *wt*. In the *wt* enzyme, Y94 is part of a H-bond network containing water molecules, H147, C146, and N5 of H_4folate. In Y94F, there is no electron density at the locations of the mutated hydroxyl and

[*] $^{D}K_{eq}$ = 1 would lead to H5/H6 ratio of 0.5 so 0.5*1.01/0.51 = 0.99.

water 608. It is suggested that delocalized water molecules now occupy that space. It is also apparent that H147 in the *wt* has more than one conformation (from partial electron density), while Y94F only adopts a single conformation. This is the most substantial effect on the whole network of H-bonding at the active site.

Proton Abstraction

The substrate dUMP, labeled with tritium at C5, is commonly used to measure the enzyme's activity (4). The use of tritium release from [5-^{3}H]-dUMP to measure the reaction rate relies on the assumption that there is no effective (observed) KIE on that step. This assumption is substantiated by the fact that the proton abstraction is not rate limiting in the overall reaction (4,10) and by the ordered nature of the *wt* TS reaction. The intrinsic KIE of step 5 in Scheme 1 has never been measured before (to the best of our knowledge). Previous experiments that monitored the ^{3}H/^{14}C ratio in the mixture of [5-^{3}H] dUMP and [2-^{14}C] dUMP (4,24), reported KIEs close to unity. This is probably due to the ordered binding mechanism of the *wt* TS (1) that "masked" the KIE when the labeling was on the dUMP that binds first (21,39,40). The relationship between the observed KIE on the second order rate constant $^T(V/K)$ and the KIE after the formation of the ternary complex ($^Tk_9$ in Scheme 2) is described in equation 6 (21, 27,41):

$$^T(V/K) = \frac{^Tk_9 + C_f + C_r\,^TK_{eq}}{1 + C_f + C_r} \quad [6]$$

where k_ns are the microscopic rate constants for the kinetic steps described in Scheme 2, C_r is the reverse commitment, which in the case of the current experiments is close to zero. * $^TK_{eq}$ is the equilibrium isotope effect on the proton abstraction, which is expected to be close to unity.

The forward commitment C_f is described by equation 7:

$$C_f = \frac{k_9}{k_5 + \frac{k_2k_4}{k_2 + k_3[B]}} \quad [7]$$

where [B] is the concentration of the second substrate (CH_2H_4folate in this case). As apparent from Eq 6 and Eq 7, the observed $^T(V/K)$ is dependent on the concentration of B and its observed value can change between two finite values (C_f changes from k_9/k_5 to $k_9/(k_5 + k_4)$ as [B] changes from infinity to zero). In contrast to the random mechanism, the C_f in an ordered mechanism in which A binds first follows:

$$C_f = \frac{k_9}{k_4} + \frac{k_3[B]}{k_2k_4} \quad [8]$$

In this case, the observed $^T(V/K)$ is dependent on the concentration of B and its observed value can change from unity (no KIE) to a finite value (C_f changes from infinity to k_9/k_4 as [B] changes from infinity to zero (21)).

In the current study, the observed KIEs on the proton abstraction from C5 of dUMP were measured as a function of the CH_2H_4folate concentration to ascertain the kinetic mechanism

*The reverse commitment is defined as $C_r = \frac{k_{10}}{k_{11}} + \frac{k_{10}k_{12}}{k_{11}k_{13}}$. Since C5 of dUMP is only trace labeled with tritium, k_{10} effectively represents competition between the water protons and the trace tritium. For the sake of simplicity, we follow the precedence of previous studies using [5-^{3}H]dUMP (4) and assume that the effective k_{10} is close to zero and thus C_r can be ignored in most of the following discussion. This assumption is further supported by comparison of the observed KIE at [B] = 0 (1.8, see Figure 2) with the intrinsic KIE ($^Tk_9$ = 3.2 as calculated below). The combined commitment is only 0.45, leaving little apparent contribution for *C* alone. At any rate, C_r is independent of [B] and does not affect the conclusion regarding the effect of the mutation on the reaction order.

for *wt* TS and Y94F. Figure 3 presents the observed KIEs as a function of CH_2H_4folate concentration. The observation that the observed H/T KIE for the *wt* approaches unity at high concentration of CH_2H_4folate (1.02 ± 0.02 at 1 mM CH_2H_4folate) while Y94F goes to an asymptote at a finite value (1.10 ± 0.02) indicates that the *wt* binding mechanism is strictly ordered (within experimental error and in agreement with previous studies (1)), but that of the mutant is more random (21). Also, the observed KIEs for the *wt* and Y94F are similar at zero [B] (1.86 ± 0.10 and 1.96 ± 0.15, respectively; Figure 3). This last observation, together with the intrinsic KIEs (see below), indicates a similar commitment on $^{T}(V/K)$ for the *wt* and the mutant.

To access the intrinsic KIE on the proton transfer step, we measured the D/T KIE at a low CH_2H_4folate concentration and then assessed the intrinsic KIE using the Northrop method (25–27). A concentration of 5 μM CH_2H_4folate was used to assure sufficient conversion of radioactive labeled dUMP on one hand, and large observed KIE values (small relative error) due to a small commitment on the other hand. The intrinsic H/T KIE on the proton abstraction for the *wt* and Y94F are practically the same (3.25 ± 0.31 and 3.17 ± 0.22, respectively, Table 1).*

Summary of the proton abstraction step

(step 4 or 4’ in Scheme 1): An intrinsic KIE of the C5 proton abstraction from dUMP is determined here for the first time. The intrinsic KIEs for both the mutant and the *wt* are similar ($^{T}k \approx 3.2$) suggesting that the effect of Y94 mutation on this transformation was too small to be detected. Apparently, while the Y94F mutation reduced the order of binding by increasing the rate of dUMP release from the ternary complex (k_5), it did not affect the actual proton transfer step. As apparent from Figure 3, the level of kinetic complexity that masks the intrinsic KIE ($^{T}k_9$) on the second order rate constant $^{T}(V/K)$ at zero CH_2H_4fole appears to be small and similar for both *wt* and the mutant ($C \approx 0.45$).#

The relatively small intrinsic KIE is in accordance with a pre-activated C5-H bond and an asymmetric transition state for this transformation (35). QM/MM calculations (via collaboration with Moliner and co-workers) are underway to quantitatively examine this observation.

Hydride Transfer

The intrinsic KIEs on the hydride transfer step (step 6 in Scheme 1) were measured and compared with the *wt* using CH_2H_4folate labeled with H, D, or T at its *R*-C6 position as described in ref (10). Since in this part, only the hydride was isotopically labeled, all the other kinetic steps are not isotopically sensitive and the kinetic equations used are not different from those used for any other system with a single isotopically sensitive step. Figure 5 shows both the temperature dependence of the observed and intrinsic KIEs of the *wt* and Y94F. The analysis of the temperature dependence of intrinsic KIEs proceeded by exponential fitting of the data to the Arrhenius equation for KIEs:

$$k_L/k_T = A_L/A_T \exp\left[(E_T - E_L)/\mathrm{RT}\right] \quad [9]$$

where k_L/k_T is L/T KIE with L representing the light isotopes, A_L/A_T is the isotope effect on preexponential factors, and $E_T - E_L$ is the isotope effect on activation energy. The biphasic behavior of the intrinsic KIEs for the mutant (Figure 5B) suggested an intrinsic phase transition

*At zero [B], C_f is k_9/k_4 for the *wt* and $k_9/(k_5 + k_4)$ for the mutant (see Eq. 7). Since C_f can also be calculated using the independently measured intrinsic KIE, it is tempting to calculate all the microscopic rate constants in Scheme 2. However, k_4 and k_9 do not have to be the same for both enzymes, and k_9 is likely to be much faster in the *wt*. Consequently the current data are insufficient for extraction of all the microscopic rate constants.

#Where $C = C_f + C_r$ and $^{T}K_{eq}$ is close to unity.

(42,43) so the data were fitted at temperature ranges of 40 – 20 °C and 20 – 5 °C independently. Above 20 °C, the KIE was temperature independent (E_T -E_H = −0.03 ± 0.30 kcal/mol) and the ratio of the Arrhenius preexponential factors (Table 2) are well above the semiclassical values (44–46). At lower temperature range, the KIEs were temperature dependent and the KIE on the Arrhenius preexponential factors were inverse (A_H/A_T<1) and below the semi-classical limits (Table 2).

Whether the temperature dependence of the KIEs can be understood within the framework of tunneling correction to transition state theory (35,45) depends on the assessment of the activation parameters on the reaction rate. To assess the activation parameters for the hydride transfer step at the high and low temperature ranges, it is necessary to extract the rates of that chemical step ($k_{hydride}$) at each temperature range. We used the method developed by Klinman and coworkers (47,48):

$$k_{hydride} = \frac{k_{cat}\left({}^{D}k - 1\right)}{{}^{D}k_{cat} - 1} \quad [10]$$

where $k_{hydride}$ is the unknown rate of the hydride transfer step; ${}^{D}k$ is the intrinsic H/D KIE for this step at each temperature (see Figure 5B) and ${}^{D}k_{cat}$ is the H/D KIE for k_{cat} using C6 labeled CH_2H_4folate. To assess the activation parameters for the two temperature regimes, k_{cat} was measured at 5, 20 and 40 °C, equation 10 was used to assess $k_{hydride}$ (Table 3). The Arrhenius equation was used to calculate E_a for the physiological and the low temperature ranges (3.1 and 6.2 kcal/mol, respectively - Table 2).

The activation energy at the physiological temperature range, together with the temperature independent intrinsic KIEs suggested that, as with the *wt*, a Marcus-like model (46,49–52) is needed to explain the findings for Y94F (10). In such a model, the rate for hydrogen tunneling arises from the combination of two terms: one is non-isotopically sensitive but determines most of the temperature dependence of the rates, and the other (depicted as the Franck-Condon term (49)) is isotopically sensitive and includes a tunneling contribution and classical fluctuations between donor and acceptor. The tunneling in such a model is dominated by the symmetry of the vibration levels (reorganization energy λ and driving force ΔG^0, the referred to "rearrangement" term in Marcus theory) and by the fluctuations of the distance between donor and acceptor, referred to as "gating") (49,51). According to the Marcus-like model, lack of temperature dependence for both *wt* and Y94F at higher temperature range, indicates ideal prearrangement of the donor and acceptor prior to tunneling, which eliminates the effect of thermally activated "gating". The comparison of Y94F to *wt* suggests that the hydride transfer for both proceeds with a similar "environmentally coupled tunneling" (50) at the physiological temperature range. However, at lower temperature, the increase of the Y94F activation energy relative to the *wt* ($\Delta E_{a\ Y94\text{-}wt}$ is about 2.8 kcal/mol) suggests a poorly pre-organized reaction coordinate and substantial need for "gating" (46,49,50).

Examination of the activation parameters in Table 2 results in an interesting observation: Most of the reduction in activity caused by the mutation appears to be on the entropy of activation ($\Delta T\Delta S^{\ddagger}$). The change in enthalpy of activation, $\Delta\Delta H^{\ddagger}$,was estimated to be 0.9 kcal/mol while -$\Delta T\Delta S$‡ was about 3.9 kcal/mol at 25 °C. Similar results were also observed for mutants of dihydrofolate reductase (36), but it is not clear at this stage how general this phenomenon is. We hope that attracting the community's attention to these observations will lead to more data collection addressing the effect of mutations on activation parameters, and maybe to a better rationalization of this phenomenon.

The relationship between the observed and intrinsic KIEs can be extracted from Eq. 6 (27, 46). At 20 °C, the observed H/T KIE on *V/K* of Y94F was measured to be 2.62 ± 0.01, while the intrinsic value is 4.86 ± 0.18, resulting in a commitment of 1.39 for the hydride transfer

step. By contrast, the hydride transfer in the *wt* is commitment free (commitment close to zero) at room temperatures (10). The inflated commitment of the observed KIE on *V/K* for Y94F indicates that this hydride transfer step is no longer commitment free (rate limiting) and that a preceding step becomes rate limiting for this mutant.

Summary of the hydride transfer step

(step 6 in Scheme 1): The Y94F exhibits biphasic behavior, with temperature independent KIEs at physiological temperature and a steep temperature dependency under 20 °C (Figure 5). At physiological temperatures, the intrinsic KIEs were as temperature independent as the *wt*. This is in accordance with conservation of the internal dynamics and coupling of the environment to the hydride transfer step (46,50), indicating only a minor role for the Y94 in step 6. At reduced temperature, the substantial temperature dependency of the KIEs with Y94F indicates a poorly pre-organized reaction coordinate and a need for thermal gating of the donor-acceptor distance (46,50).

The phenomenon of intrinsic phase transition of this type has been previously reported for thermophilic enzymes (42,43,46) but not yet for a mesophilic enzyme. A possible explanation for the phase transition at 20 °C for Y94F (Figure 5) is that the removal of the "anchored" Tyr 94 hydroxyl and the lack of localization of the water molecule closest to C5 of dUMP (red ball in Figure 4) disrupts the H-bond network at the active site. This, in turn, may alter the structural and dynamic properties of that network (which serves as the acceptor for the C5 proton), leading to a poorly preorganized reaction coordinate and a longer effective donor-acceptor distance at reduced temperature (46,50).

Kinetic analysis – Which step(s) is affected by the Y94F mutation?

Observations

1. Hydride transfer is rate limiting for both *V/K* and k_{cat} in *wt* (the commitments on both rate constants is close to zero). In contrast, for Y94F both k_{cat} and *V/K* for dUMP are masked (the observed KIEs are smaller than the intrinsic KIEs due to non-zero commitment). This indicates that the mutation affects a kinetic step that is part of both rate constants- e.g., the affected kinetic step is between the formation of the ternary complex and the first irreversible step. Specifically:
    a. For Y94F, the inflated commitment (relative to the *wt*) for the hydride transfer's $^{T}(V/K)$ indicates that the step affected by mutation precedes the hydride transfer.
    b. For Y94F, there is a small difference in commitment for the second order rate constant $^{T}(V/K)$ of proton transfer, which indicates a small effect of mutation on the preceding steps, suggesting that most of the effect is after the proton abstraction.
2. The intrinsic KIEs for the proton transfer (using [5-^{3}H]-dUMP) are the same for *wt* and Y94F. This result suggests that the mutation does not affect the proton abstraction step per sé.
3. The K_M for dUMP is not affected by mutation but the K_M for CH_2H_4folate is increased (19). This is in accordance with random binding for the mutant, which is proposed here based on the dependence of the observed KIEs for proton abstraction as function of CH_2H_4folate concentration.
4. Santi, D.V., Schultz P.G. and co-workers (19) examined relevant mutants (Y146 in *L. casei* TS) as catalysts for CH_2H_4folate-independent dehalogenation of [5-Br]-dUMP, a reaction which simulates early steps of the normal pathway up to and

including enzyme-nucleotide covalent adduct formation. Many of these mutants had activity comparable to the wild-type enzyme, indicating that the effects of the mutations occur after the initial covalent adduct is formed.

Interpretation—The effect of the mutation on steps that precede the formation of the ternary complex and proton abstraction is small, and mostly reflects the reduced binding capacity of dUMP (larger k_5 in Scheme 2). Most of the effect is on a step(s) that take place between the two H-transfer steps, specifically steps 5 or 5' in Scheme 1. Possible events that may occur along step 5 are deprotonation of the enolate in C4 and/or protonation of N5 of the H_4folate leaving group. Possible events that may occur along step 5' are deprotonation of the thiol (if protonated during the elimination step 4') and/or protonation of N5 of the H_4folate leaving group.

CONCLUSIONS

A new insight into the chemical mechanism of the thymidylate synthase catalyzed reaction is presented. Many studies have proposed that a conserved active site tyrosine (Y94 in *ec*TS) serves as a general base that enhances proton abstraction during the elimination of H_4folate (step 4 in Scheme 1; for review see ref (4)). The effect of the Y94F mutation on two distinct chemical steps has been examined. These steps were the proton abstraction step (step 4 in Scheme 1) and the hydride transfer step (step 6 in Scheme 1). The findings indicate that the proposed tyrosine (Y94, 3.6 Å from the proton donor) is not the main contributor to the proton abstraction step, but rather the whole network of H-bonds at the active site appears to serve as the general base. This conclusion is in accordance with the proposal of Hardy and coworkers (20) who used 5-deazatetrahydrofolate and concluded that N5 of H_4folate contributes to this general base. Additional candidates away from C5 are the imidazole and carboxylate side chains of H147 (5–6 Å) and E58 (~7 Å). Out of these we prefer the closer and more basic imidazole group. Future work will examine the H147V mutant and the *wt* TS from *B. subtilis*, which has a Val rather than His in that position. It is of course possible that no single functional group exclusively constitutes the general base, but all three contribute to the basicity of the initial proton acceptor (a water oxygen).

What accounts for the two order of magnitude decrease in Y94F activity relative to the *wt* TS? Taken together, the findings suggest that at physiological temperature the step most affected by the mutation occurs after the proton abstraction and prior to the hydride transfer. According to the mechanism illustrated in Scheme 1, these are likely to be step 5 or step 5', specifically the protonation of N5 of H_4folate (in both paths) or the deprotonation of the enol in step 5. Additionally, the mutation weakens the binding and enhances the release of dUMP, which results in a random binding sequence (Scheme 2). QM/MM calculations comparing this mutant to the *wt* (16) are underway and may offer a molecular insight into the findings reported here.

Acknowledgment

The authors are grateful to Drs. Judith Klinman, Paul Cook, and Dexter Northrop for fruitful and helpful discussions.

References

1. Carreras CW, Santi DV. The catalytic mechanism and structure of thymidylate synthase. Annu. Rev. Biochem 1995;64:721–762. [PubMed: 7574499]
2. Phan J, Steadman DJ, Koli S, Ding WC, Minor W, Dunlap RB, Berger SH, Lebioda L. Structure of human thymidylate synthase suggests advantages of chemotherapy with noncompetitive inhibitors. J. Biol. Chem 2001;276:14170–14177. [PubMed: 11278511]

3. Sergeeva OA, Khambatta HG, Cathers BE, Sergeeva MV. Kinetic properties of human thymidylate synthase, an anticancer drug target. Biochem. Biophys. Res. Commun 2003;307:297–300. [PubMed: 12859954]
4. Finer-Moore JS, Santi DV, Stroud RM. Lessons and conclusions from dissecting the mechanism of a bisubstrate enzyme: Thymidylate synthase mutagenesis, function, and structure. Biochemistry 2003;42:248–256. [PubMed: 12525151]and many cited there in
5. Stroud RM, Finer-Moore JS. Conformational dynamics along an enzymatic reaction pathway: Thymidyate synthase, "the movie". Biochemistry 2003;42:239–247. [PubMed: 12525150]
6. Saxl RL, Reston J, Nie Z, Kalman TI, Maley F. Modification of *Escherichia coli* thymidylate synthase at tyrosine-94 by 5-Imidazolylpropynyl-2'- deoxyuridine 5'-monophosphate. Biochemistry 2003;42:4544–4551. [PubMed: 12693951]
7. Maley F, Pedersen-Lane J, Changchien L. Complete restoration of activity to inactive mutants of *Escherichia coli* thymidylate synthase: Evidence that *E. coli* thymidylate synthase is a half-the-sites activity enzyme. Biochemistry 1995;34:1469–1474. [PubMed: 7849005]
8. Saxl RL, Changchien L-M, Hardy LW, Maley F. Parameters affecting the restoration of activity to inactive mutants of thymidylate synthase via subunit exchange: Further evidence that thymidylate synthase is a half-of-the-sites activity enzyme. Biochemistry 2001;40:5275–5282. [PubMed: 11318651]
9. Lorenson MY, Maley GF, Maley F. The purification and properties of thymidylate synthetase from chick embryo extracts. J. Biol. Chem 1967;242:3332–3344. [PubMed: 6067595]
10. Agrawal N, Hong B, Mihai C, Kohen A. Vibrationally enhanced hydrogen tunneling in the *E. coli* thymidylate synthase catalyzed reaction. Biochemistry 2004;43:1998–2006. [PubMed: 14967040]
11. Newby Z, Lee TT, Morse RJ, Liu Y, Liu L, Venkatraman P, Santi DV, Finer-Moore JS, Stroud RM. The role of protein dynamics in thymidylate synthase catalysis: variants of conserved 2'-deoxyuridine 5'-monophosphate (dUMP)-binding Tyr-261. Biochemistry 2006;45:7415–7428. [PubMed: 16768437]
12. Phan J, Mahdavian E, Nivens MC, Minor W, Berger S, Spencer HT, Dunlap RB, Lebioda L. Catalytic cysteine of thymidylate synthase is activated upon substrate binding. Biochemistry 2000;39:6969–6978. [PubMed: 10841779]
13. Hyatt DC, Maley F, Monfort WR. Use of strain in a stereospecific catalytic mechanism: crystal structures of *Escherichia coli* thymidylate synthase bound to FdUMP and methylenetetrahydrofolate. Biochemistry 1997;36:4585–4594. [PubMed: 9109668]
14. Spencer HT, Villafranca JE, Appleman JR. Kinetic scheme for thymidylate synthase from *Escherichia coli*: determination from measurements of ligand binding, primary and secondary isotope effects and pre-steady-state catalysis. Biochemistry 1997;36:4212–4222. [PubMed: 9100016]
15. Hong B, Haddad M, Maley F, Jensen JH, Kohen A. Hydride transfer versus hydrogen radical transfer in thymidylate synthase. J. Am. Chem. Soc 2006;128:5636–5637. [PubMed: 16637621]
16. Kanaan N, Martí S, Moliner V, Kohen A. A quantum mechanics/molecular mechanics study of the catalytic mechanism of the thymidylate synthase. Biochemistry 2007;46:3704–3713. [PubMed: 17328531]
17. Matthews DA, Villafranca JE, Janson CA, Smith WW, Welsh K, Freer S. Stereochemical mechanism of action for thymidylate synthase based on the X-ray structure of the covalent inhibitory ternary complex with 5-Fluoro-2'-deoxyuridylate and 5,10-methylenetetrahydrofolate. J. Mol. Biol 1990;214:937–948. [PubMed: 2201779]
18. Fauman EB, Rutenber EE, Maley GF, Maley F, Stroud RM. Water-mediated substrate/product discrimination: the product complex of thymidylate synthase at 1.83 Å. Biochemistry 1994;33:1502–1511. [PubMed: 8312270]
19. Liu Y, Barrett JE, Schultz PG, Santi DV. Tyrosine 146 of thymidylate synthase assists proton abstraction from the 5-position of 2'-deoxyuridine 5'-monophosphate. Biochemistry 1999;38:848–852. [PubMed: 9888826]
20. Hardy LW, Graves KL, Nalivaika E. Electrostatic guidance of catalysis by a conserved glutamic acid in *Escherichia coli* dTMP synthase and bacteriophage T4 dCMP hydroxymethylase. Biochemistry 1995;34:8422–8432. [PubMed: 7599133]

21. Cook, PF. Enzyme mechanism from isotope effects. Cook, PF., editor. Boca Raton, FL.: CRC Press; 1991. p. 203-230.
22. Pogolotti AL, Weill C, Santi DV. Thymidylate synthetase catalyzed exchange of tritium from [5-^{3}H]-2'-deoxyuridylate for protons of water. J. Am. Chem. Soc 1979;18:2794–2798.
23. Carreras CW, Climie SC, Santi DV. Thymidylate synthase with a Cterminal deletion catalyzes partial reactions but is unable to catalyze thymidylate formation. Biochemistry 1992;31:6038–6044. [PubMed: 1627546]
24. Huang W, Santi DV. Isolation of a covalent steady-state intermediate in glutamate 60 mutants of thymidylate synthase. J. Biol. Chem 1994;269:31327–31329. [PubMed: 7989294]
25. Northrop DB. Steady-state analysis of kinetic isotope effects in enzymatic reactions. Biochemistry 1975;14:2644–2651. [PubMed: 1148173]
26. Northrop, DB. Isotope effects on enzyme-catalyzed reactions. Cleland, WW.; O'Leary, MH.; Northrop, DB., editors. Baltimore, MD: University Park Press; 1977. p. 122-152.
27. Northrop, DB. Intrinsic isotope effects in enzyme catalyzed reactions. In: Cook, PF., editor. Enzyme mechanism from isotope effects. Boca Raton, FL: CRC Press; 1991. p. 181-202.
28. Cleland, WW. Enzyme mechanisms from isotope effects. In: Kohen, A.; Limbach, HH., editors. Isotope effects in chemistry and biology. Boca Raton, FL: Taylor & Francis, CRC Press; 2006. p. 915-930.
29. Blakley RL. Crystalline dihydropteroylglutamic acid. Nature 1960;188:231–232.
30. Agrawal N, Mihai C, Kohen A. Microscale synthesis of isotopically labeled *R*-[6-$^{\times}$H]-N5,N10-methylene 5,6,7,8-tetrahydrofolate as a substrate for thymidylate synthase. Anal. Biochem 2004;328:44–50. [PubMed: 15081906]
31. Hayatsu H, Wataya Y, Kai K, Iida S. Reaction of sodium bisulfite with uracil, cytosine, and their derivatives. Biochemistry 1970;9:2858–2865. [PubMed: 5459538]
32. Wataya Y, Hayatsu H. Cysteine-catalyzed hydrogen isotope exchange at the 5 position of uridylic acid. J. Am. Chem. Soc 1972;94:8927–8928. [PubMed: 4639922]
33. Wataya Y, Hayatsu H. Effects of amine on the bisulfite-catalyzed hydrogen isotope exchange at the 5 position of uridine. Biochemistry 1972;11:3583–3588. [PubMed: 5053761]
34. Changchien L-M, Garibian A, Frasca V, Lobo A, Maley GF, Maley F. High-level expression of Escherichia coli and Bacillus subtilis thymidylate synthase. Prot. Expres. Pur 2000;19:265–270.
35. Melander, L.; Saunders, WH. Krieger, RE. Reaction rates of isotopic molecules. 4th ed. Malabar, FL: 1987.
36. Wang L, Tharp S, Selzer T, Benkovic SJ, Kohen A. Effects of a distal mutation on active site chemistry. Biochemistry 2006;45:1383–1392. [PubMed: 16445280]
37. Cleland WW. Measurement of isotope effects by the equilibrium perturbation technique. Methods in Enzymol 1980;64:104–125. [PubMed: 7374451]
38. Roberts SA, Hyatt DC, Honts JE, Changchien L, Maley GF, Maley F, Montfort WR. Structure of the Y94F mutant of *Escherichia coli* thymidylate synthase. Acta Cryst 2006;F62:840–843.
39. Klinman JP, Humphriesg H, Voe JG. Deduction cf kinetic mechanism in multisubstrate enzyme reactions from tritium isotope effects. J. Biol. Chem 1980;255:11648–11651. [PubMed: 7002926]
40. Cook PF, Cleland WW. Mechanistic deductions from isotope effects in multireactant enzyme mechanisms. Biochemistry 1981;20:1790–1796. [PubMed: 7013799]
41. Cleland, WW. Secondary isotope effectson enzymatic reactions. In: Buncel, E.; Lee, CC., editors. Isotopes in organic chemistry. Amsyerdam: Elsevier; 1987. p. 61-113.
42. Kohen A, Cannio R, Bartolucci S, Klinman JP. Enzyme dynamics and hydrogen tunneling in a thermophilic alcohol dehydrogenase. Nature 1999;399:496–499. [PubMed: 10365965]
43. Maglia G, Allemann RK. Evidence for environmentally coupled hydrogen tunneling during dihydrofolate reductase catalysis. J. Am. Chem. Soc 2003;125:13372–13373. [PubMed: 14583029]
44. Stern MJ, Weston REJ. Phenomenological manifestations of quantummechanical tunneling. II. Effect on Arrhenius pre-exponential factors for primary hydrogen kinetic isotope effects. J. Chem. Phys 1974;60:2808–2814.
45. Bell, RP. The tunnel effect in chemistry. London, UK and New York, NY: Chapman & Hall; 1980.

46. Kohen, A. Kinetic isotope effects as probes for hydrogen tunneling in enzyme catalysis. In: Kohen, AL.; H, H., editors. Isotope Effects in Chemistry and Biology. Boca Raton, FL: Taylor & Francis - CRC Press; 2006. p. 743-764.

47. Francisco WA, Knapp MJ, Blackburn NJ, Klinman JP. Hydrogen tunneling in peptidylglycine α-Hydroxylation monooxygenase. J. Am. Chem. Soc 2002;124:8194–8195. [PubMed: 12105892]

48. Miller SM, Klinman JP. Secondary isotope effects and structure-reactivity correlations in the dopamine β-monooxygenase reaction: Evidence for a chemical mechanism. Biochemistry 1985;24:2114–2127. [PubMed: 3995006]

49. Knapp MJ, Klinman JP. Environmentally coupled hydrogen tunneling linking catalysis to dynamics. Eur. J. Biochem 2002;269:3113–3121. [PubMed: 12084051]

50. Nagel ZD, Klinman JP. Tunneling and dynamics in enzymatic hydride transfer. Chem. Rev 2006;106:3095–3118. [PubMed: 16895320]

51. Wang L, Goodey NM, Benkovic SJ, Kohen A. Coordinated Effects of Distal Mutations on Environmentally Coupled Tunneling in Dihydrofolate Reductase. Proc. Natl. Acad. Sci. USA 2006;103:15753–15758. [PubMed: 17032759]

52. Marcus RA. H and other transfers in enzymes and in solution: theory and computations, a unified view. 2. applications to experiment and computations. J. Phys. Chem. B 2007;111:6643–6654. [PubMed: 17497918]

53. Kohen A. Kinetic isotope effects as probes for hydrogen tunneling, coupled motion and dynamics contributions to enzyme catalysis. Prog. React. Kin. Mech 2003;28:119–156.

1. Abbreviations and Textual footnotes

TS, thymidylate synthase; KIE, kinetic isotope effect; RP HPLC, Reverse Phase High Pressure Liquid Chromatography; LSC, Liquid Scintillation Counter; dUMP, 5-FdUMP 5-fluoro- 2'-deoxyuridine-5'-monophosphate; 2'-deoxyuridine-5'-monophosphate; dTMP, 2'-deoxythymidine-5'-monophosphate; CH_2H_4folate, N^5, N^{10}-methylene 5,6,7,8 tetrahydrofolate; H_2folate, 7,8-dihydrofolate; H_4folate, 5,6,7,8-tetrahydrofolate.

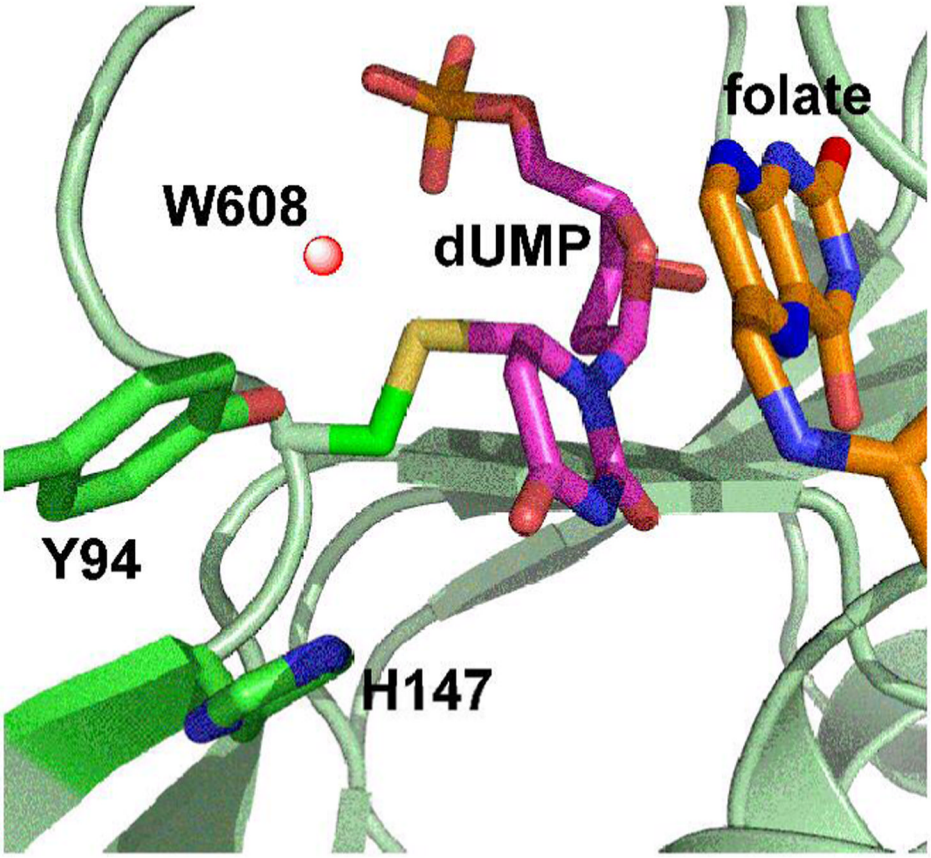

Figure 1.
Structure of *wt E. coli* TS covalently bound to dUMP (PDB code 2KCE) with Y94 and H147 highlighted in green, the water molecule closest to the Y94 (1.7 Å) and to C5 of the dUMP is highlighted as a red ball, the dUMP in magenta is covalently bound to C146, and the pterin ring is in orange.

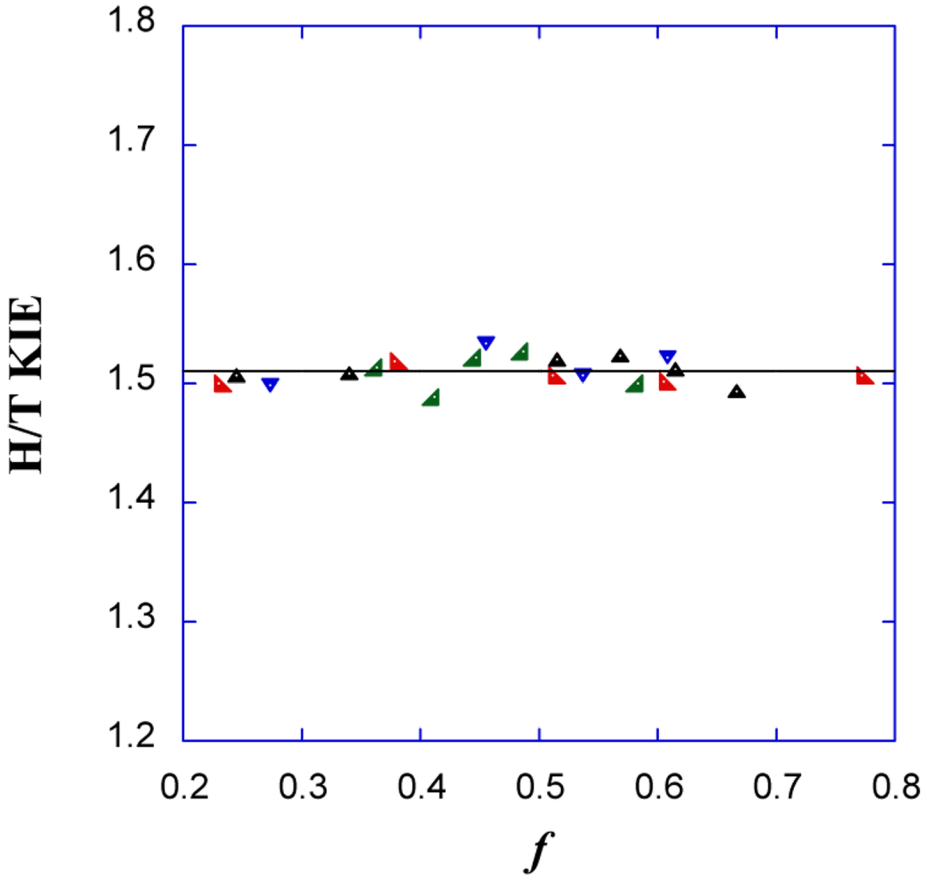

Figure 2.

H/T KIEs as function of fractional conversion as measured for *wt* TS at 25 °C in 5 μM CH_2H_4folate. The different colors and shapes represent points measured in four independent experiments. The average value is 1.52 ± 0.03 and no upward or downward trend is observed within statistical error.

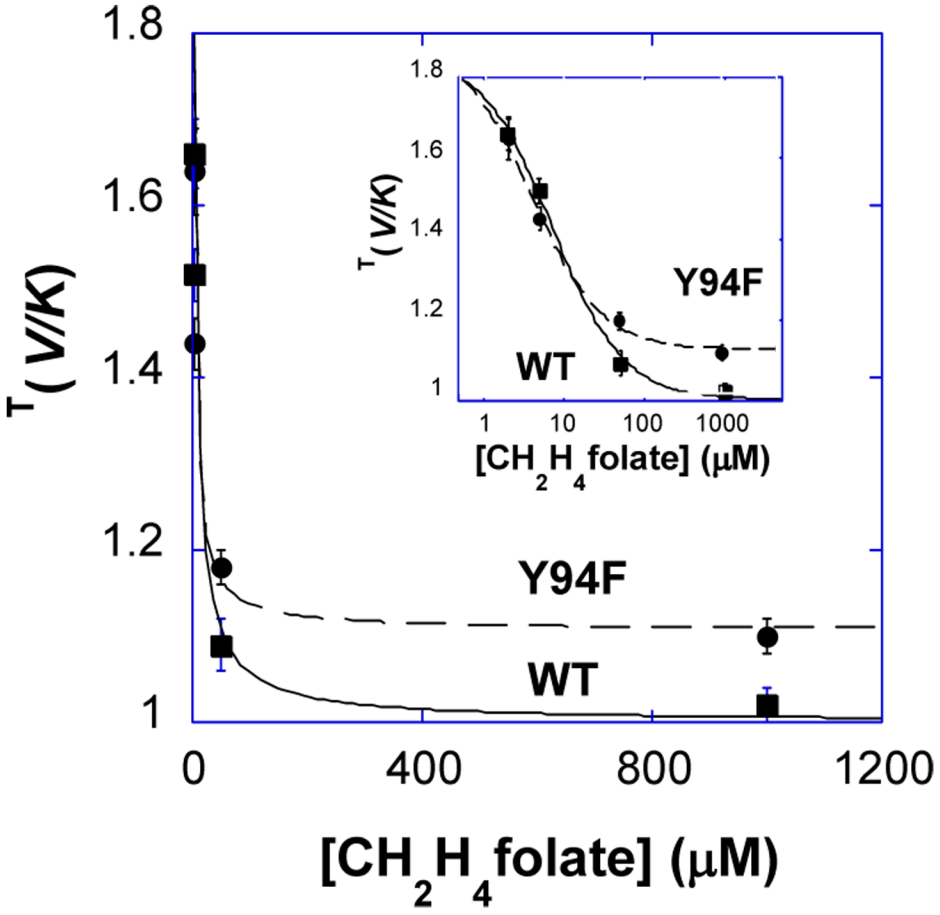

Figure 3.
H/T KIE for proton abstraction as a function of CH_2H_4folate concentration. Data with Y94F (circles) and with *wt* (squares) are compared. Solid and dashed lines are fits to Eq. 6 for the *wt* and the Y94F, respectively.

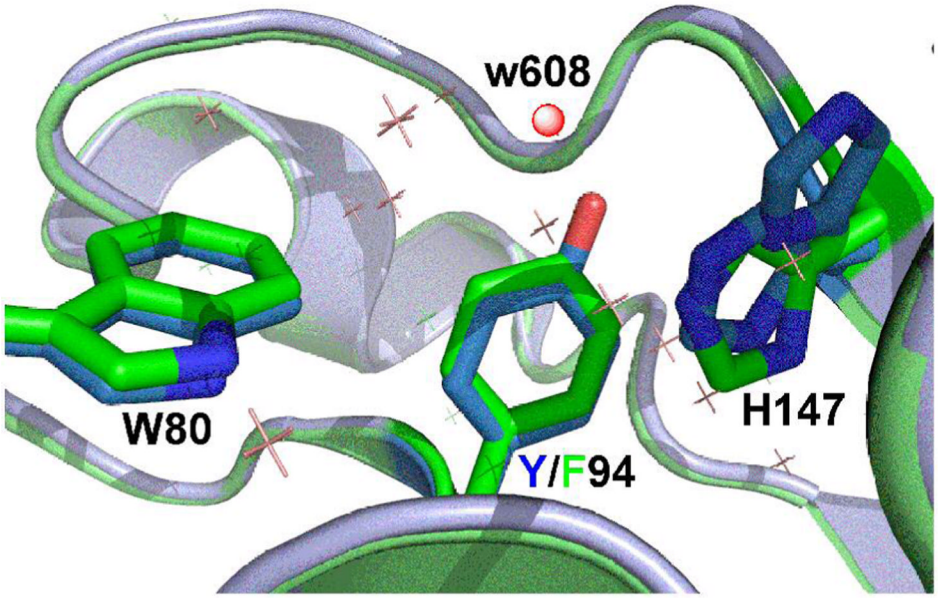

Figure 4.

wt TS (blue - PDB ID # 2FTQ) and Y94F (green - PDB ID # 2FTN) with Y/F94, W80, and H147 presented as sticks. The water molecule closest to the Y94 (w608, 2.6 Å from its O) is highlighted as red ball and is missing in the mutant. All other water molecule are marked by crosses and practically overlap for the *wt* and the mutant. See also Figure 3 in ref (38). Note that the two-fold orientation of H147 is only apparent in the *wt* (blue), but not in Y94F (green).

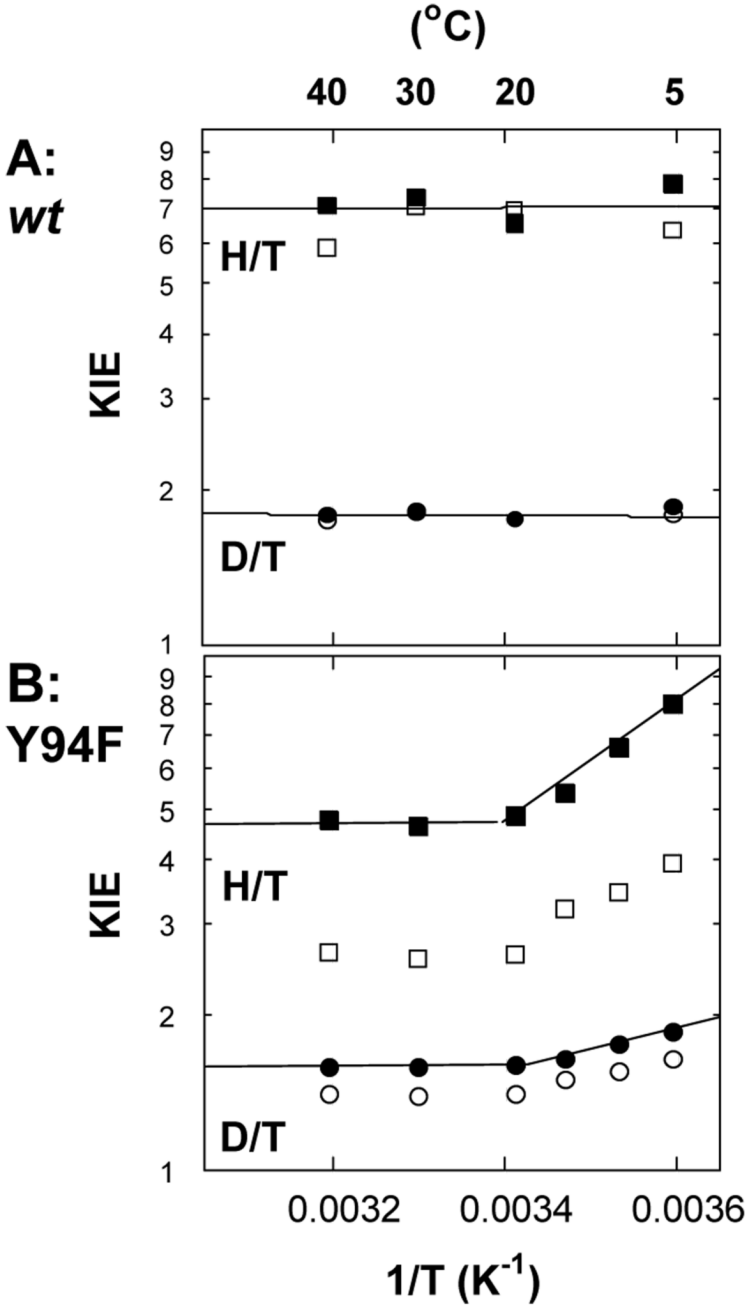

Figure 5.
Arrhenius plots of observed (empty structures) and intrinsic (filled structures) primary H/T KIEs (squares) and primary D/T KIEs (circles). The lines are the exponential fittings of the intrinsic KIEs to Eq. 5. A. *wt*. and B. Y94.

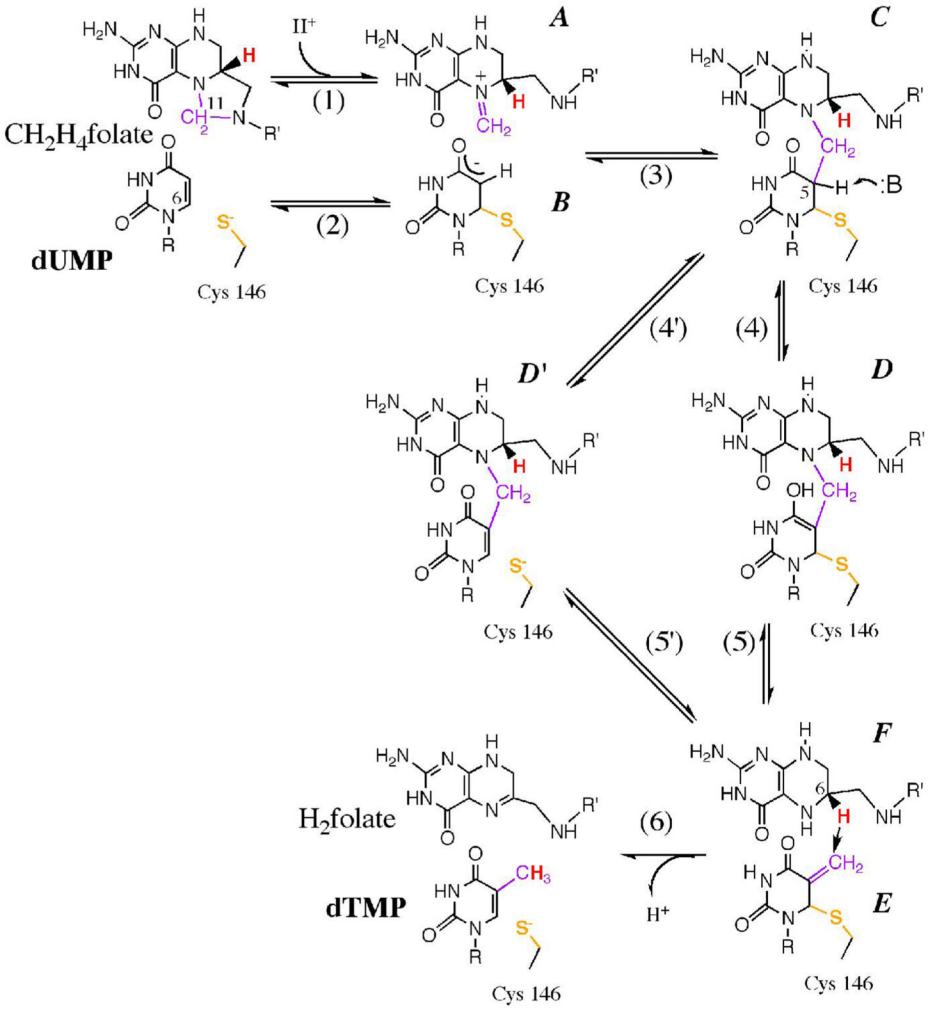

Scheme 1.
The proposed chemical mechanisms of the TS catalyzed reaction.

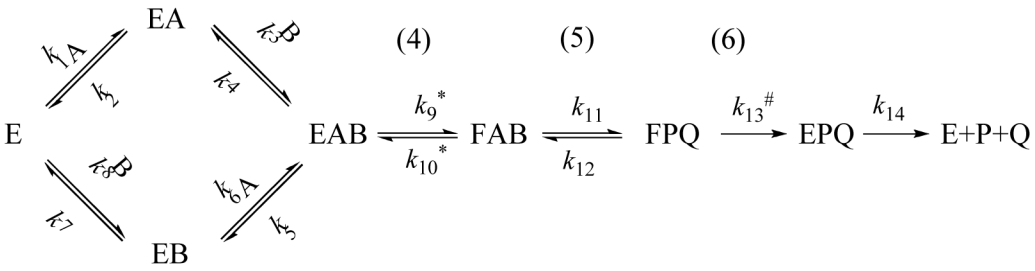

Scheme 2.

Binding scheme for a sequential mechanism. In this case, A represents dUMP and B represents CH_2H_4folate. The relevant steps from Scheme 1 are presented in parenthesis. Rate constants that are isotopically sensitive in the proton abstraction experiments (using labeled dUMP) are marked with * and the one that is isotopically sensitive in the hydride transfer experiments (using labeled CH_2H_4folate) is marked with #.

Table 1

Kinetic isotope effect of the wild-type and Y94F TS on proton abstraction at 25 °C.

KIE	Wild Type	Y94F
$^{T}(V/K)H^{a}$	1.52 ± 0.03	1.44 ± 0.03
$^{T}(V/K)D^{a}$	1.17 ± 0.01	1.15 ± 0.01
H/T KIE_{int}	3.2 ± 0.2	3.2 ± 0.3
D/T KIE_{int}	1.41 ± 0.03	1.42 ± 0.04
H/D KIE_{int}	2.2 ± 0.1	2.3 ± 0.2

[a] At 5 μM CH_2H_4folate.

Table 2

Rates and isotope effect on Arrhenius parameters of the wild-type and Y94F TS on hydride transfer[a].

	Wild type[b]	Y94F		SC A_L/A_T[c]
	5 – 40 °C	**5 – 20 °C**	**20 – 40 °C**	
A_H/A_T	6.9 ±1.0	0.0002 ±0.0001	4.5 ±0.5	0.5 –1.6
A_D/A_T	1.8 ±0.1	0.07 ±0.02	1.6 ±0.1	0.9 –1.2
ΔE_{aH-T}	0.02 ±0.09	6.0 ±0.5	0.03 ±0.40	
ΔE_{aD-T}	0.01 ±0.02	1.8 ±0.2	0.06 ±0.12	
E_a	4.0 ±0.3	6.2 ±0.3	3.1 ±0.1	
$\Delta H^{\ddagger}$	3.4 ±0.08	5.6 ±0.3	2.5 ±0.1	
$T\Delta S^{\ddagger}$25°C	−13.7 ±0.7	−14.5 ±0.5	−17.6 ±0.7	

[a] All energy units are kcal/mol.

[b] From ref. (10).

[c] Semi-classical limits of isotope effects on preexponential factor of Arrhenius equation.(35,45,46,53).

Table 3

Observed k_{cat} and $^{T}k_{cat}$ used to assess the values of $k_{hydride}$ at 5, 20, and 40 °C using Eq. 10[a].

wild type[b]		Y94F		
Temp. [°C]	**k_{cat} [s^{-1}]**	**k_{cat} [s^{-1}]**	**$^{D}k_{cat}$**	**$k_{hydride}$ [s^{-1}]**
40	1.6	0.0067	2.24	0.0109
20	1.1	0.0055	2.36	0.0080
5	0.73	0.0023	4.20	0.0026

[a] All relative errors are under 2 % of the measured values and under 6 % of the calculated $k_{hydride}$.

[b] From ref. (10).